SANDIA REPORT

SAND2006-0152
Unlimited Release
Printed February 2006

Progress Toward a MEMS Fabricated 100 GHZ Oscillator

P. Dale Coleman, Guillermo Loubriel, Thomas Lemp, James E. Rowley, and Mark Weyn

Prepared by
Sandia National Laboratories
Albuquerque, New Mexico 87185 and Livermore, California 94550

Sandia is a multiprogram laboratory operated by Sandia Corporation, a Lockheed Martin Company, for the United States Department of Energy's National Nuclear Security Administration under Contract DE-AC04-94AL85000.

Issued by Sandia National Laboratories, operated for the United States Department of Energy by Sandia Corporation.

Available to DOE and DOE contractors from
U.S. Department of Energy
Office of Scientific and Technical Information
P.O. Box 62
Oak Ridge, TN 37831

Telephone: (865)576-8401
Facsimile: (865)576-5728
E-Mail: reports@adonis.osti.gov
Online ordering: http://www.osti.gov/bridge

Available to the public from
U.S. Department of Commerce
National Technical Information Service
5285 Port Royal Rd
Springfield, VA 22161

Telephone: (800)553-6847
Facsimile: (703)605-6900
E-Mail: orders@ntis.fedworld.gov
Online order: http://www.ntis.gov/help/ordermethods.asp?loc=7-4-0#online

SAND2006-0152
Unlimited Release
Printed February 2006

Progress Toward a MEMS Fabricated 100 GHZ Oscillator

P. Dale Coleman, Guillermo Loubriel
Directed Energy Special Applications Department, 5133

Thomas Lemp
Photonic Microsystems Technology, 1713

Mark Weyn
Development Builds, 27221
Sandia National Laboratories
P.O. Box 5800
Albuquerque, New Mexico 87185-1153

James E. Rowley
SAIC
2109 Airpark Rd SE
Albuquerque, New Mexico 87106

Abstract

This report summarizes an LDRD effort which looked at the feasibility of building a MEMS (Micro-Electro-Mechanical Systems) fabricated 100 GHz micro vacuum tube.

PIC Simulations proved to be a very useful tool in investigating various device designs. Scaling parameters were identified. This in turn allowed predictions of oscillator growth based on beam parameters, cavity geometry, and cavity loading.

The electron beam source was identified as a critical element of the design. FEA's (Field Emission Arrays) were purchased to be built into the micro device. Laboratory testing of the FEA's was also performed which pointed out care and handling issues along with maximum current capabilities.

Progress was made toward MEMS fabrication of the device. Techniques were developed and successfully employed to build up several of the subassemblies of the device. However, the lower wall fabrication proved to be difficult and a successful build was not completed.

Alternative approaches to building this structure have been identified. Although these alternatives look like good solutions for building the device, it was not possible to complete a redesign and build during the timeframe of this effort.

Acknowledgments

Several colleagues contributed to this report. Thanks go to Guillermo Loubriel for his extensive management and technical input to the project. Much valued input also came from Dave Seidel, Vince Hietala, Mike Wanke, and Albert Baca. Mark Weyn's many hours of effort in FEA testing are also much appreciated. Special thanks go to Jed Rowley for his countless PIC simulation runs. Finally, thanks go to Tom Lemp for his determined efforts on the MEMS front and for his input to the MEMS section of this report.

Contents

Figures

Introduction

This work was motivated in part by desires for a non-lethal option when addressing hostile combatants. High-frequency RF has been shown to create a strong flee reaction. However, present systems designed for this RF application are based on vacuum tube technology and, thus, are expensive, large, and fragile. Further, conventional semiconductors do not have the required power. This LDRD proposed to build a MEMS fabricated micro vacuum electronic source that could be arrayed to yield a robust, high power, and relatively inexpensive alternative to present systems. These sources could find uses in access denial (military and civilian use), higher resolution SARs, wideband communications, and imaging through obscurants (including clothing and epoxies used in weapons manufacturing).

As a proof of principle first step, a single oscillator was deigned, modeled, and progress was made toward building the first device. This document reviews various aspects of the project and summarizes results and conclusions.

Device Concept

A transit time oscillator (TTO) was chosen as the initial demonstration device (shown below).

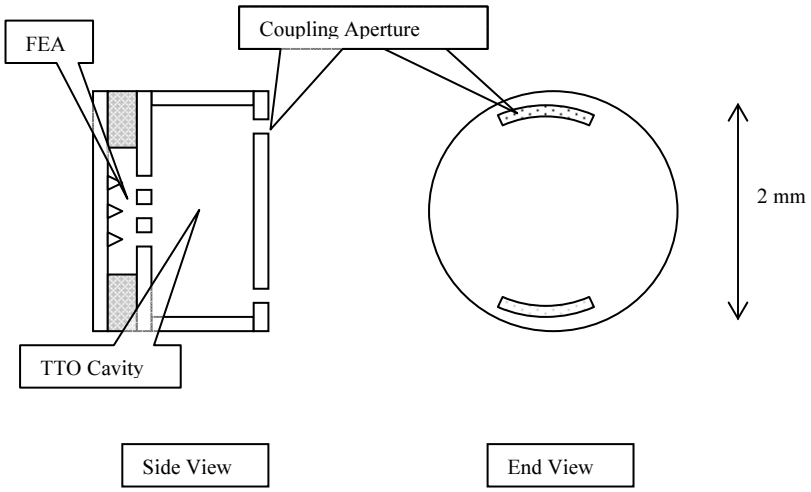

Figure 1 Schematic of first prototype Transit Time Oscillator (TTO).

The TTO consists of a pillbox cavity through which and electron beam passes exciting oscillations (1,2,3,4). If the electron is in the cavity long enough for the field to reverse sign, then on average, the beam loses energy, and the RF fields grow. Small coupling apertures in the downstream plate of the prototype system allow radiation of the RF.

A commercial field emission array (FEA) was to be used to generate the working electron beam (5). The design called for the cavity structure to be diffusion bonded onto the FEA's platform. Lithography, thin film, electroplating, and diffusion bonding techniques were to be carried out in a class 100 clean room environment.

Transit Time Oscillator (TTO) Theory

The basic TTO configuration consists of a beam being injected along the axis of a simple pill box resonant cavity. Under the proper conditions the electron's kinetic energy can feed the growth of the rf electric field.

Consider a beam crossing a gap on which a uniform electric field E is imposed. If one solves for the equation of motion and averages over an rf period, it can be shown that under appropriate conditions, the beam will on average loose kinetic energy to the field.

In the small signal limit, the electric field oscillation grows as

$$E = E_0 \cdot e^{t/\tau_b} .$$

It can be shown that the growth rate, $1/\tau_b$, scales as

$$\frac{1}{\tau_b} \propto \frac{I}{V} \cdot (R/Q) \cdot f(\theta) .$$

Where I is the beam current; V is the beam voltage; R is the cavity shunt impedance, Q is the cavity quality factor and (R/Q) is a cavity geometry function that represents how concentrated the electric field is in the region of the beam; and $f(\theta)$ is an oscillatory function of the particle transit angle (see figure below)

$$f(\theta) = \frac{\theta \sin\theta - 2(1-\cos\theta)}{\theta^2} .$$

The transit angle θ is given by

$$\theta = \omega d / v .$$

With ω being the rf angular frequency, d is the axial gap extent, and v the particle velocity.

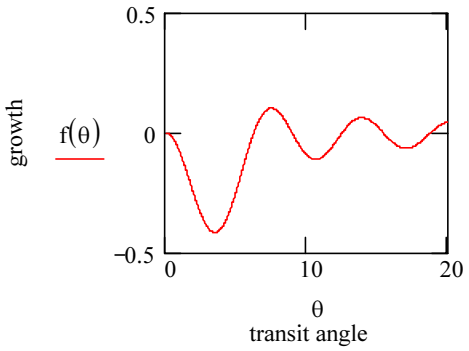

Figure 2 Calculation showing growth rate dependence on transit angle.

Note the oscillation grows when f(θ) is positive with the first region of growth occurring around $\theta = 2.4\,\pi$.

The big advantage to the TTO is its simplicity (to build and to analyze). However, its primary disadvantage is that it has a slow growing instability. Because of this, any damping (wall losses, external loading, etc.) must be kept to a minimum to insure the instability grows.

TTO Simulations

Extensive simulations of the device have been performed using Two Quick, a 2D particle in cell (PIC) code. The figure below shows typical output from the code. Shown are four examples of the on axis electric field growing at different rates.

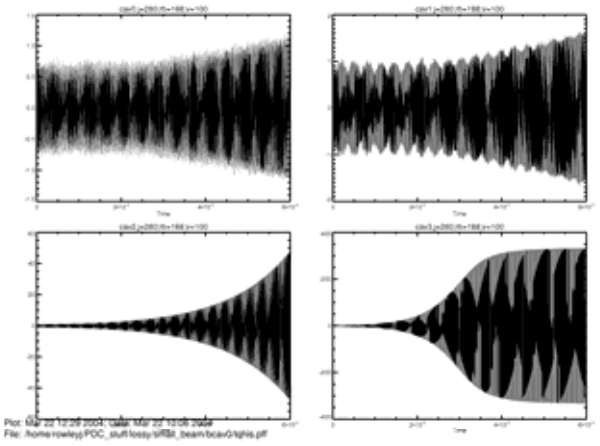

Figure 3 PIC simulation output showing examples of different growth rates as the cavity geometry is varied. (R/Q) = 11, 15, 23, 53 for the upper left, upper right, lower left and lower right cases respectively. Higher (R/Q)'s are seen to result in faster growth rates.

Various parameters affecting oscillator performance are discussed below.

Growth Studies

A series of parameter scans were performed to determine the sensitivity of instability growth to various cavity and beam parameters.

Beam Parameters

The instability growth rate showed no strong dependence with current density (see below).

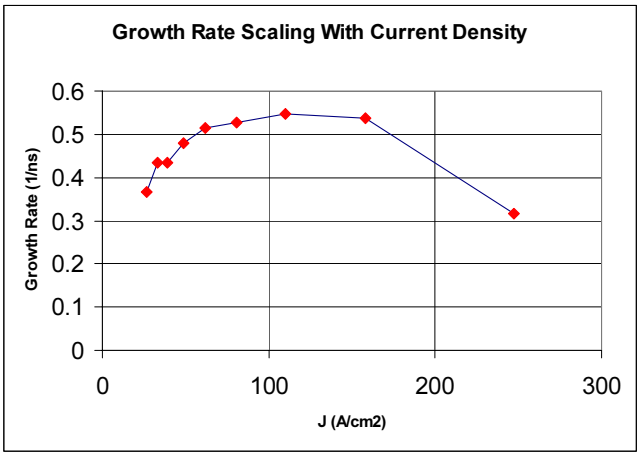

Figure 4 TTO growth rate dependence on current density. Parameters of Scan: 23Mar04 run, V=100 V, I=310 mA, varied beam radius.

However, simulations clearly show that growth rate was linearly dependent on beam current and inversely dependent on beam voltage (shown below)

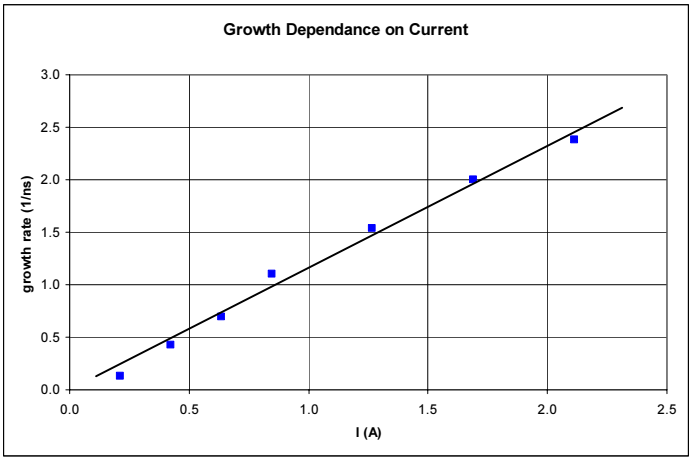

Figure 5 TTO growth rate dependence on beam current. Parameters of Scan: 19 Feb04 run, pillbox cavity, rbeam = 508 μm, V=100 V.

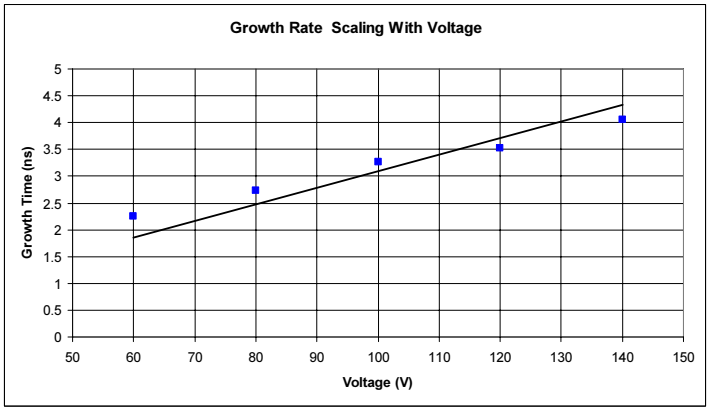

Figure 6 TTO growth time (1/growth rate) dependence on beam voltage. Parameters of Scan: 10Mar04 run, J=40 A/cm2, rbeam=500 μm, pillbox cavity, axial extent of cavity varied with voltage to keep transit time resonance satisfied

Cavity Parameters

The instability growth rate is also seen to be a function of the cavity geometry.

The TTO Theory discussed earlier predicts as the axial extent of the cavity, and hence the transit angle, is changed one should see multiple resonances. The chart below shows the occurrence of the first two resonant conditions.

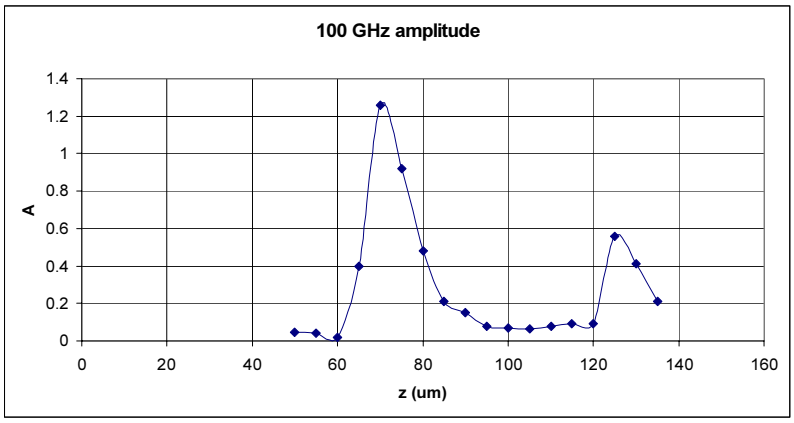

Figure 7 Dependence of TTO growth rate on axial extent of cavity.

The growth rate is also enhanced if the cavity geometry is modified to be reentrant which increases the electric field in the region of the beam. The figure below shows the reentrant geometry

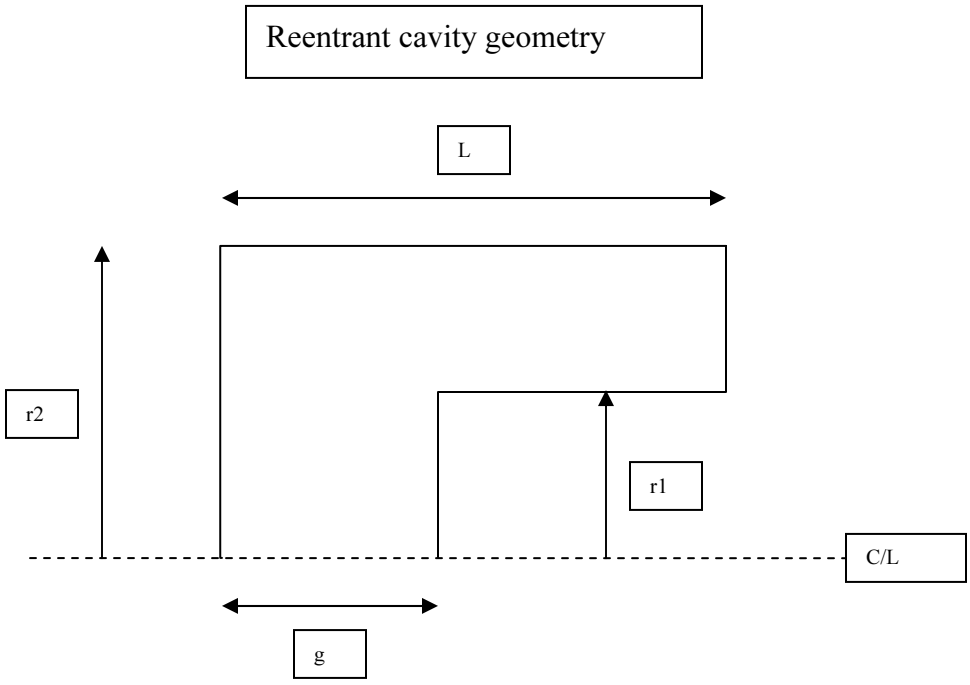

Figure 8. Reentrant cavity geometry.

This enhance growth rate comes at the expense of having to build a more complicated cavity geometry. This modification of the geometry can be quantified with the parameter (R/Q), where R is the cavity shunt impedance and Q is the cavity quality factor. Growth rate scaling with (R/Q) is shown below.

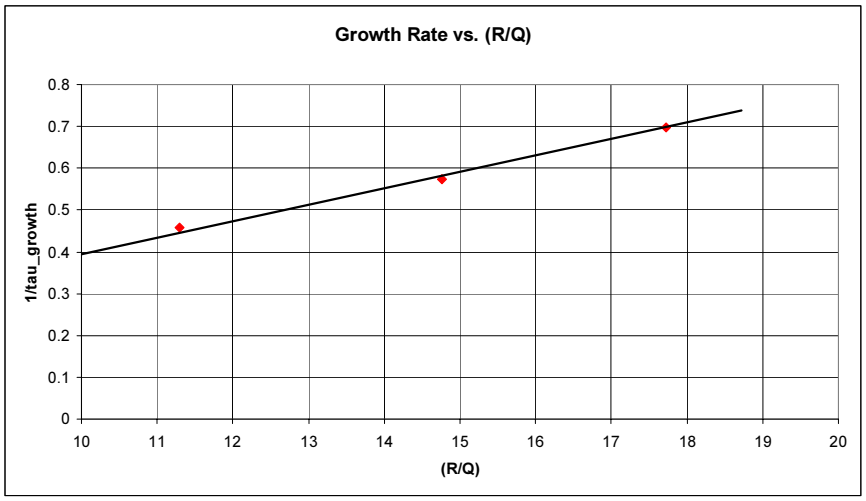

Figure 9 TTO growth rate dependence on cavity R/Q. Scan Parameters: pillbox and two reentrant geometries, rb=500 um, V=100 V, I=310 mA

Cavity Loading Studies

The growth rate scaling studies discussed above assumed no loading of the oscillator. The use of a 2D code required compromise on how to model a three dimensional iris loaded cavity. To mock up the aperture loading, a bulk conductivity (σ) is applied to the cavity volume and is varied to adjust the degree of loading. In addition to this conductivity loading a small amount of numeric damping is in place to address computational stability.

The observed growth rate scales as

$$\frac{1}{\tau_g} = \frac{1}{\tau_n} + \frac{1}{\tau_\sigma} + \frac{1}{\tau_b} = \frac{1}{\tau_{loaded}} + \frac{1}{\tau_b}$$

Therefore, for net positive growth of the instability, the unloaded instability growth rate ($1/\tau_b$) must be larger than the applied loading.

Loading of the cavity is characterized by exciting a cold cavity (no particles but finite σ) and measuring the field decay time (τ_{loaded}):

$$E = E_0 \cdot e^{-t/\tau_{loaded}}$$

Data for three different geometry cavities, a pill box and two reentrant versions, are plotted below. The table summarizes the cavity geometry and some figures of merit.

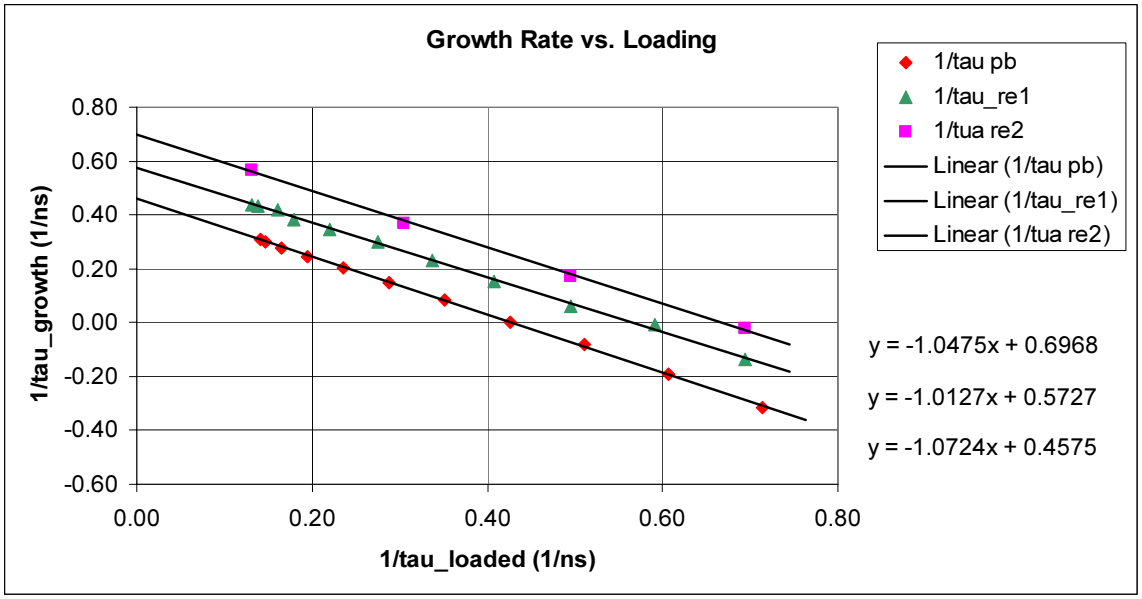

Figure 10 Loading effects on TTO growth rates. Parameters of scan: V=100 V, I=310 mA, rbeam=500 μm.

cavity	r1 (μm)	r2 (μm)	L(μm)	g (μm)	R/Q	$1/\tau_{crit}$ (ns^{-1})	Q_{crit}	Q_{Cu}
pill box	1150	1150	70	70	11.29	0.43	731	316
re #1	600	790	220	70	14.76	0.57	551	476
re #2	500	705	260	70	17.72	0.67	469	539

The horizontal axis represents how heavily the cavity is damped. The vertical axis represents how fast the instability grows (or decays if it is negative).

When damping is light ($1/\tau_{loaded}$ is small) the instability grows quickly (large positive $1/\tau_{growth}$). As the damping is increased (τ_{loaded} gets smaller) the growth of the oscillations slows. When $1/\tau_{growth}$ is 0, the damping is just strong enough to keep the instability from growing.

In an actual cavity, the total loading will come from two main sources: radiation out the iris and wall losses. Therefore, in order to radiate any RF, the instability has to be able at a minimum to overcome wall losses. Copper cavity wall losses have been calculated for each cavity type and are listed in the above table in terms of Q_{Cu} .

For the pillbox case, critical damping occurs when $1/\tau_{loaded} = 0.43$ ($Q_{crit} = \omega\tau/2 = 731$). So if the cavity Q is < 731 the instability will not grow. Unfortunately, for a copper cavity, the Q due to wall resistivity is 316, so there is no hope of getting the oscillation to grow.

However, efficiency increases if one tries to improve the beam's interaction with the cavity fields by making the geometry a reentrant one. Now the critical $1/\tau_{loaded}$ = 0.57 or Q_{crit} = 551. Now for this geometry, the Cu cavity Q = 476. Closer to a growing instability, but not quite there.

The reentrant#2 cavity has a Cu cavity Q = 539 and a critical Q = 469. Now the instability is seen to still be able to grow in the presence of the cavity wall losses. Indeed this design shows the most promise for successfully radiating RF from the device.

So what if one makes the geometry more reentrant. This would indeed help. However, as the cavity becomes more reentrant, the reentrant post diameter shrinks to a radius less than that of the beam (r = 500 μm). At this point the device would start to suffer added inefficiencies since not all the beam would be in the interaction region.

SCO Simulations

The above analysis indicated that, for typical beam parameters available from Field Emission Arrays (FEA's) and for the simple baseline cavity geometry, the TTO instability was weak. As a result, overcoming wall losses could be problematic. A Split Cavity Oscillator, SCO, (4) cavity design was investigated as a second generation device that could possibly provide a more robust instability. A figure showing the SCO geometry is shown below.

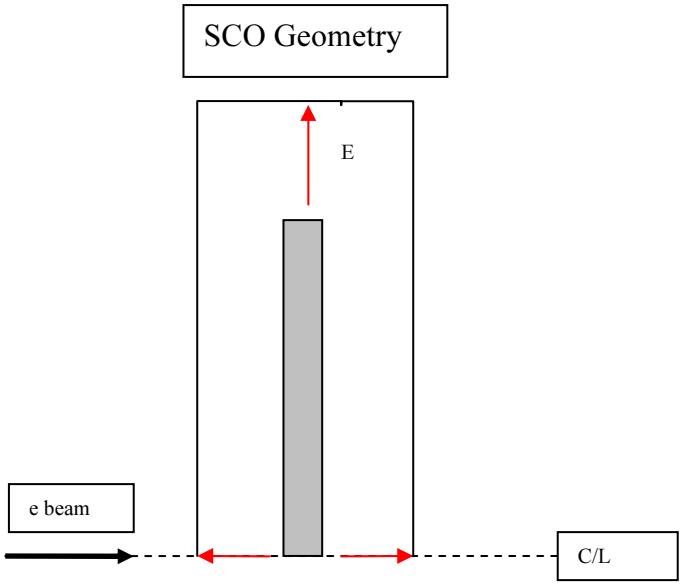

Figure 11 SCO geometry.

A conducting grid located at the cavity midplane divides the cavity into tow regions. This cavity structure supports a transverse magnetic mode that has the electric field 180º out of phase in the adjacent regions. Under the proper conditions, an injected beam interacts unstably with this mode causing it to grow at the expense of the beam's kinetic energy.

Extensive PIC simulations were performed to optimize the cavity geometry. Instability growth rates were calculated for various beam currents and beam radii.

The Figure below shows a scan of axial gap extent.

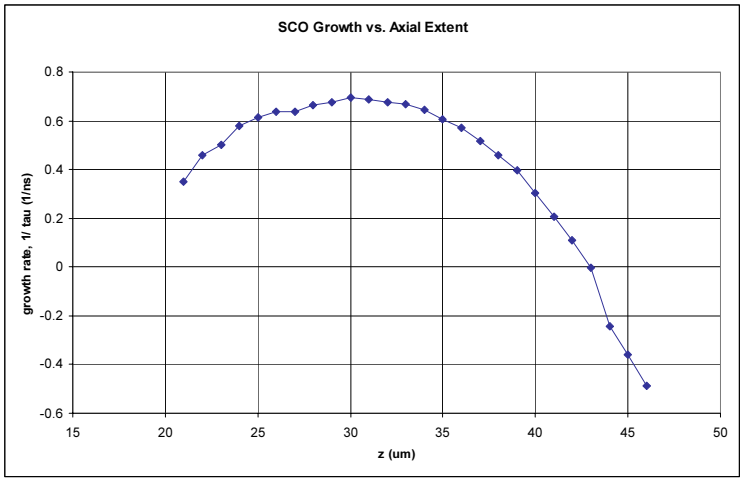

Figure 12 SCO growth rate dependence on axial gap extent.

The data show that the optimum axial half gap is approximately 30 μm (i.e. total axial extent of the SCO structure is 60 μm) .

The instability growth as a function of beam current is shown below.

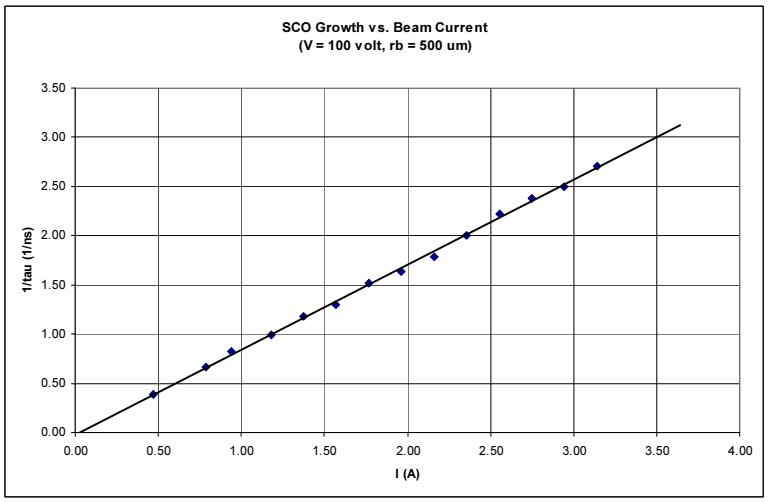

Figure 13 SCO growth rate dependence on beam current.

Just as in the previous cavity geometries considered, the growth rate is seen to scale linearly with current. Although oscillations were well defined, excessive currents (beyond the capabilities of the FEA) were again required to overcome wall losses.

FEA Testing Results

Self contained FEA devices were procured from SRI International and tested. This allowed familiarization of the handling and operation of this type electron source before it was incorporated into the final TTO package.

Test Configuration

The photos below show a close up of the FEA (mounted in a T05 case for testing purposes) and the vacuum chamber used in testing the FEA's .

Figure 14 Photographs of the commercial FEA and the test bed used for studying the FEA's V-I characteristics.

Measured V-I curves

The circuit below was used to map V-I curves for the test FEA's.

Micro-Vacuum RF Device Technology

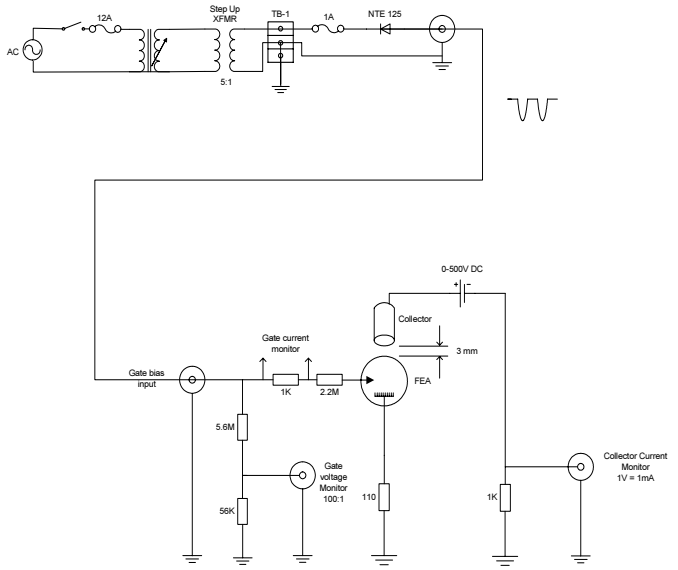

FEA initial turn on/warm up circuit configuration

Figure 15 Schematic of circuit used to map V–I curve for FEA's.

The chart below displays a measured V-I curve relative to that expected (based on SRI data). The roll off of current at higher voltages is attributed to contamination of the FEA. These devices are extremely sensitive to ion bombardment of tips and hence require very high vacuums and very careful handling procedures.

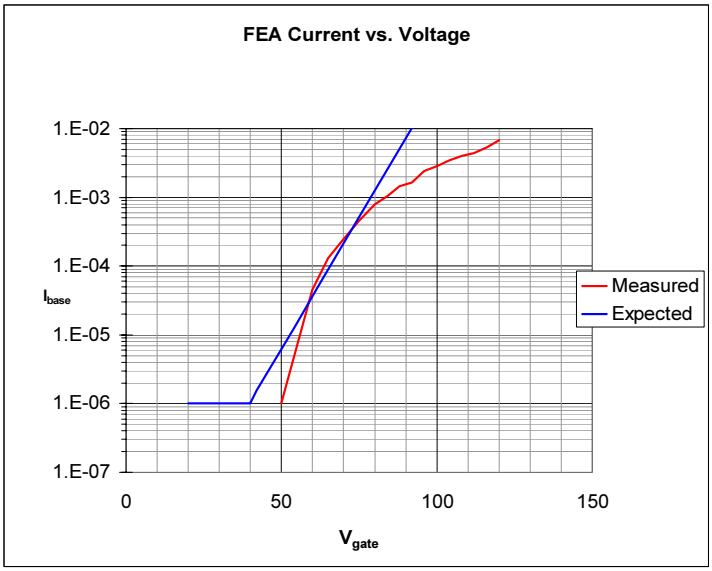

Figure 16 Measured FEA performance compared to expected results.

Typical currents achieved in these test were 10's of mA. The maximum performance demonstrated by SRI thus far is a 300 mA, 100 V beam. The scaling studies discussed above all indicate that a higher current, lower voltage beam is advantageous for oscillation growth. The capabilities of the FEA are marginal at best and other cathode approaches should be considered.

MEMS Fabrication

The pillbox TTO design was seen as the simplest structure and was hence chosen as the first prototype to build. The figure below depicts the design of the intended device. Fabrication of this device can be conveniently separated into five subassemblies: the substrate with sealed electrically conductive vias, the FEA fabrication, the lower wall fabrication including the pocket that locates and stabilizes the FEA prior the brazing it in place; the top fabrication including the top electrical FEA contact, diffusion bonding locating ring, and antenna ports (irises).

Figure 17 MEMS TTO design using pillbox resonant cavity.

The substrate is a clear dielectric LiSi2O5 ceramic 1 mm thick. Vias were laser drilled and filled with a conductive low firing temperature Ag/Cu material. The substrates were lapped flat, cleaned, and Au pads were electro-formed on both sides of the vias to provide electrical contacts, mechanical stability, and hermeticity if the finished device were to be sealed in a vacuum. The substrate was successfully built.

FEA fabrication, initial testing, and pre-delivery packaging were done by SRI International as a collaborative effort. Testing was done in TO5 headers; however, the die was not bonded in the package, but vacuum packaged as a removable die. The intended use of the die was to fit it into a gold pocket on the substrate, hold it in place with the deformable top contacts that would provide a 74 micron standoff to the top plate/antenna, and braze it in place with the same operation that diffusion bonds the top in place. The FEA location pocket was successfully fabricated.

The top of the device is designed in two layers on LiSi2O5 from which it is released once bonded into place. The outside rim of the top rides over the side wall of the lower wall and is thus self aligning. The outside rim is 74 microns high as is the inner FEA contact ring. The inner ring has 4 small arc sections removed to aid

pump out upon diffusion bonding and to allow some definable areas for deformation upon contact to the FEA.
The top plate which the rings attach to has 4 narrow irises cut in the top which act as antennas. Various designs were used to study for efficacy. The top was successful fabricated.

The lower wall was to be the height of the FEA and brazing pad plus 74 microns (750 microns high). This wall is separated from the FEA retaining structure to the extent that the bare LiSi2O5 between the wall and pad will hold off 500 volts between the FEA bottom and top. The wall thickness is defined as 200microns.

This is a particular area of difficulty. The defined process is a series of 200 micron high negative resist definitions where each defined trench is filled, lapped, and iteratively defined and plated again. The difficulty is in defining resist structures on top existing resist and lapped metal. Numerous experiments were run and a good procedure for how to produce this structure has been identified. However, this was not the case when the processing for this device was done. The structure is too narrow to be effectively processed as it was intended to be processed at the time. Residual resist and lapping residue was problematic. A redesign would require a minimum of 4 new masks to enable this device to be processed using resist as originally intended.

An alternative would be define the FEA pocket in PMMA (polymethyl methacrylate) with an X-ray mask and exposure and then to bond PMMA on those existing lapped structures and the remaining 1st layer of PMMA. The latter process and the associated details have been defined and proven as a result of another development effort. This second alternative does not require a redesign, or additional masks. It does require additional processing of the existing substrates, but less total processing than the original design has required; this is partially due to the fact that the wall can be produced utilizing one layer of PMMA. The LIGA group has certainly struggled producing this tall 'lower' wall.

This Microwave device is complex: it requires tight dimensions, tall structures, and 7 mask layers. Unique development was required for producing the vias in LiSi2O5, the FEA, the lower wall, and the integration of these layers. Although the device can now be produced with some process modifications, we were not successful at the time it was funded.

Discussion

Summary of Simulations

PIC Simulations proved to be a very useful tool in investigating various device designs. Scaling parameters were identified. This in turn allowed predictions of oscillator growth based on beam parameters, cavity geometry, and cavity loading.

Detailed loading calculations led to the conclusion that the TTO and SCO instabilities are weak enough that just overcoming wall loses will be problematic. Using a more complicated reentrant TTO design was seen to improve the device efficiency.

Cathode Considerations

Sample FEA's were tested in the lab. It was found that successful operation of these devices required careful attention to avoid contamination of the array.

Simulations indicate that higher beam currents would lead to faster growing instabilities. However the current FEA capabilities (300 mA over the 1μm diameter) are marginal at best for the oscillator designs considered thus far.

Stronger oscillations could be achieved if higher values of I/V could be reached. Other cathodes, such as carbon naotubes (6), should be investigated to see if they can provide more attractive beam parameters:

MEM's Considerations.

Progress was made toward MEMS fabrication of the device. Techniques were developed and successfully employed to build up several of the subassemblies of the device. However, the lower wall fabrication proved to be difficult. The structure was found to be too narrow to be effectively processed as it was intended. Residual resist and lapping residue was problematic.

Alternative approaches to building this structure have been identified. Although these alternatives look like good solutions for building the device, it was not possible to complete a redesign and build during the timeframe of this effort.

Alternate Oscillator Designs

A pillbox TTO geometry was initially considered because of its simplicity. It was found that a more complicated reentrant design would be required in order to overcome wall losses. The SCO was also found to lack in its performance.

In order to achieve robust operation, it may be beneficial to investigate more complicated oscillator designs such as a reflex klystron (7).

References

1. J. Marcum, J. Appl. Phys., vol. 17, p4, 1946
2. J. W. Luginsland, et. al., “High-power transit-time oscillator: Onset of oscillation and saturation”, Phys. Plasmas, Vol. 4, No. 12, Dec. 1997.
3. M. Mostrom et. al., “Proton-Beam Transit-Time Oscillator”, Mission Res. Corp., Albuquerque, NM, Tech. Rep. MRX/ABQ-R-1030, 1988
4. B. Marder, et. al., “The Split-Cavity Oscillator”, IEEE Trans on Plasma Sci, Vol. 20, No. 3, 1992.
5. C. A. Spindt, et. al, “Field-Emitter Arrays for Vacuum Microelectronics”, IEEE Trans. on Electron Dev., Vol 38, No. 10. Oct 1991.
6. S. H. Jo, et. al., “Effect of length and spacing of vertically aligned carbon nanotubes on field emission properties”, App. Phys. Let., Vol. 82, No. 20, May 2003.
7. A. S. Gulmour, Jr., Microwave Tubes, Artech House, 1986, p. 235.

Distribution

External Distribution:

1 James E. Rowley
SAIC
2109 Airpark Rd SE
Albuquerque, NM 87106

Internal Distribution:

1	MS	1165	William Guyton, 5400
1		1153	Bob Turman, 5440
1		1153	Malcolm Buttram, 5446
5		1153	Guillermo Loubriel, 5443
5		1153	Dale Coleman, 5443
1		1153	Larry Bacon, 5443
1		1153	Robert Salazar, 5443
1		1153	Fred Zutavern, 5443
1		1033	Vince Hietala, 1712
1		0344	Tom Lemp, 1713
1		0344	John Williams, 1713
1		0603	Mike Wanke, 1713
1		0603	Albert Baca, 1742
1		1152	Dave Seidel, 1652
1		9018	Central Technical Files, 8945-1
2		0899	Technical Library, 4536